Miniature Protein Ligands for EVH1 Domains: Interplay between Affinity, Specificity, and Cell Motility†

Jennifer H. Holtzman,‡ Kamil Woronowicz,§ Dasantila Golemi-Kotra,§ and Alanna Schepartz*,‡,§

Department of Chemistry and Department of Molecular, Cellular and Developmental Biology, Yale University, New Haven, Connecticut 06520

Received May 21, 2007; Revised Manuscript Received August 8, 2007

ABSTRACT: Dynamic rearrangements of the actin cytoskeleton power cell motility in contexts ranging from intracellular microbial pathogenesis to axon guidance. The Ena/VASP family proteins—Mena, VASP, and Evl—are believed to control cell motility by serving as a direct link between signaling events and the actin cytoskeleton. It has previously been reported that a novel miniature protein, pGolemi, binds with high affinity to the EVH1 domain of Mena ($Mena_{1-112}$) but not to those of VASP ($VASP_{1-115}$) or Evl (Evl_{1-115}) and also causes an unusual defect in actin-driven *Listeria monocytogenes* motility. Here, scanning mutagenesis was used to examine the effects of single amino acid changes within pGolemi on EVH1 domain affinity and specificity, miniature protein secondary structure, and *L. monocytogenes* motility. The data suggest that pGolemi contains the expected aPP-like fold and binds $Mena_{1-112}$ in a manner highly analogous to the proline-rich repeat region of *L. monocytogenes* ActA protein. Residues throughout pGolemi contribute to both EVH1 domain affinity and paralog specificity. Moreover, the affinities of pGolemi variants for $Mena_{1-112}$ correlate with selectivity against the EVH1 domains of VASP and Evl. In *L. monocytogenes* motility assays, speed and speed variability correlate strongly with EVH1 paralog specificity, suggesting that the Ena/VASP paralogs do not play equivalent roles in the process of *L. monocytogenes* actin tail maturation.

The actin cytoskeleton is a complex system that transduces multiple converging signals into changes in the dynamics and architecture of actin assembly. An important family of direct regulators of the actin cytoskeleton, the Ena/VASP proteins are implicated in an astounding array of actin-based biological functions (*1*−*8*). These functions include the formation of cell membrane protrusions, particularly lamellipodia and filopodia, that are the hallmarks of amoeboid crawling motility in neuronal growth cones and fibroblasts during wound healing; platelet aggregation; formation of the T cell receptor immunological synapse; formation of focal adhesions and stress fibers during cell spreading; and motility of intracellular pathogens, such as *Listeria monocytogenes*.

The Ena/VASP family proteins include three paralogs in vertebrates: Mena, VASP, and Evl (*9*−*12*). These proteins share an overall three-part domain organization consisting of an N-terminal EVH1[1] domain, a central domain containing proline-rich sequences, and a C-terminal EVH2 domain (*4*, *13*). The EVH1 domain is involved in recruitment of Ena/VASPs to their site of activity by specific interaction with proline-rich sequences in its binding partners. The central domain of the Ena/VASPs contains one or more phosphorylation sites depending on the particular paralog or splice variant (*11*, *14*−*17*). This region is also rich in proline and serves as a docking site for proline recognition domains such as profilin and SH3 domains (*10*, *18*−*21*). The C-terminal EVH2 domain is responsible for multiple functions, including oligomerization of the Ena/VASPs through a coiled coil domain (*22*) and binding to both actin monomers and filaments. In VASP and Mena, EVH2 functions are modulated by phosphorylation (*16*, *23*−*26*).

Much effort has been devoted to studying the structure and function of the EVH1 domains and their interactions with proline-rich sequences (PRSs). PRSs are also recognized by several unrelated domains such as the SH3 (*27*−*29*), WW (*29*−*31*), GYF (*32*, *33*), and UEV (*34*, *35*) domains as well as the single domain protein profilin (*36*−*38*). Proline-mediated interactions tend to be low affinity (1−500 μM range) (*39*, *40*), a feature that allows macromolecular complex assembly and disassembly to respond to internal and extracellular signals on a rapid time scale. Ligands for proline recognition domains share a number of features, most importantly the ability to adopt a type II polyproline (PPII) helix that positions the cyclic pyrrolidine side chains on one helical face into grooves formed by aromatic residues in the EVH1 domain binding pocket. Contacts arising from non-proline residues that extend the core binding epitope confer specificity and augment affinity (*40*). Four classes of homologous EVH1 domains have been structurally characterized to date (*5*, *41*−*43*), and the residue preferences and binding orientation have been determined for three of these. For the EVH1 domains of Ena/VASP proteins, termed class I domains, the register or binding mode is determined by an aromatic or leucine residue in the second position of the

† This work was supported by the National Institutes of Health (GM 65453) and in part by a fellowship to J.H.H. from NSERC Canada.

* Corresponding author [telephone (203) 432-8276; fax (203) 432-3486; e-mail alanna.schepartz@yale.edu].

‡ Department of Chemistry.

§ Department of Molecular, Cellular and Developmental Biology.

[1] Abbreviations: PPII helix, type II polyproline helix; aPP, avian pancreatic polypeptide; CD, circular dichroism; K_d, dissociation constant; EVH1, Ena/VASP homology domain 1; MRE_{222}, mean residue ellipticity at 222 nm.

10.1021/bi700975f CCC: $37.00
Published on Web 11/01/2007

consensus sequence (D/E)(F/L/W/Y)PXϕPX$_{1-3}$, where X can be any amino acid and ϕ is a residue with a hydrophobic side chain. Class II EVH1 domains found in the Homer/Vesl family proteins implicated in synaptic plasticity (*44*) recognize the consensus PPxxF, although the binding orientation is the same as class I ligands. The third class is composed of WASP and N-WASP. The only known ligand for this domain is a 25-residue peptide from WIP (WASP-interacting protein) that contains an LPPPEP motif. The structure for this complex was solved using a fusion construct of the two binding partners, and the ligand orientation was opposite that of the examples mentioned above (*41*). No ligands are known for the class IV EVH1 domains found in Spred and Sprouty proteins that modulate tyrosine kinase signaling (*43*). Structural data are now available for representatives of each class of EVH1 domain (*41*−*46*), and alignment of the backbone residues shows the structures to be virtually superimposable.

Although the determinants of specificity between classes of proline recognition domains have been well studied, little is known about subtle differences between paralogs from the same class. This dearth of information arises because it is difficult to design molecules that possess sufficient specificity to discriminate between protein paralogs while retaining high affinity (*47*). Significant progress toward that goal in the context of EVH1 domain recognition was achieved with the initial characterization of pGolemi, a well-folded 30-residue polypeptide that exhibits high affinity for the Mena EVH1 domain (Mena$_{1-112}$) and high paralog specificity (*65*). pGolemi was obtained by substituting five residues from the sequence of a known EVH1 ligand, the first proline-rich repeat of the *L. monocytogenes* ActA protein, for six judiciously chosen residues of the N-terminal PPII helix and β-turn regions of avian pancreatic polypeptide (aPP). The strategy used to design pGolemi has been successfully used by our laboratory (*47*−*56*) and others (*57*−*60*) to generate high-affinity ligands for shallow surfaces that are often difficult to target using smaller molecules. The resulting miniature protein bound Mena$_{1-112}$ with high nanomolar affinity, a 10-fold improvement over the previously reported highest affinity ligand, an 11-residue peptide from ActA (ActA$_{11}$) (*42*). pGolemi bound with low affinity to the EVH1 domains of the two other Ena/VASP paralogs, VASP (VASP$_{1-115}$) and Evl (Evl$_{1-115}$), with equilibrium dissociation constants respectively 20- and >100-fold higher than that for Mena$_{1-112}$.

In addition to achieving a high level of paralog specificity, pGolemi was unique because of the dramatic effect it had on the motility of *L. monocytogenes* in cell-free extracts, a well-established system for studying the actin polymerization motor (*66*). In the presence of pGolemi, *L. monocytogenes* assumed a discontinuous actin comet tail characterized by overall slowed motility and alternating bursts and lulls in speed that correlate to bright and dark regions of the rhodamine-labeled actin tail, giving it an overall punctate appearance and the emergence of "hopping." Discontinuous comet tails during actin-based *L. monocytogenes* motility at steady state have been reported previously in cell extracts (*61*) and cultured mammalian cells (*62*) as well as in the context of ActA-coated beads in a mixture of purified proteins (*63*). A study of the process of *L. monocytogenes* motility initiation showed that hopping is a characteristic step in the establishment of robust tails to support continuous forward motion (*64*). In contrast to the effect of pGolemi, ActA$_{11}$ failed to produce discontinuous tails at any concentration tested.

In light of these results, we sought to better characterize the biochemical and structural basis for pGolemi binding, paralog specificity, and the relationship of these recognition events to the motility aberrations reported previously. To this end, a series of pGolemi variants was synthesized. Each member of the series contained a single amino acid substitution at a position expected to play a role in Mena$_{1-112}$ EVH1 binding or protein folding. The effects of these changes on binding EVH1 domain paralogs and on protein secondary structure were measured. Finally, *L. monocytogenes* motility assays were performed using a judiciously chosen set of variants to test the hypothesis that the discontinuous tail phenotype is related to pGolemi's specificity.

RESULTS

Identification of pGolemi Variants. To study the energetic contribution of individual pGolemi side chains to EVH1 affinity, specificity, and cell motility, we synthesized 18 pGolemi variants in which a single residue was substituted with alanine and used quantitative binding assays to determine the affinity of each variant for the EVH1 domains within Mena (Mena$_{1-112}$), VASP (VASP$_{1-115}$), and Evl (Evl$_{1-115}$), as detailed in the Supporting Information (*65*). We also prepared three additional variants, two in which a single proline residue at position 3 or 4 was replaced with sarcosine (abbreviated Z) and a third one containing leucine in place of Ala11. The equilibrium dissociation constants of the variant·Mena$_{1-112}$ complexes determined in this way ranged from 800 nM to >100 μM, corresponding to free energies (ΔG_{Mena}) that vary over 3 kcal·mol^{-1} (Table 1).

Recognition of Mena$_{1-112}$ by pGolemi variants. The Mena$_{1-112}$ affinity of each variant shown in Table 1 was determined using a tryptophan fluorescence perturbation assay, as described previously (*65*, *67*). The Mena$_{1-112}$ complexes formed from these variants were characterized by dissociation constants between 800 nM and >100 μM, which correspond to binding free energies between −8.3 and > −5.8 kcal·mol^{-1} (Figure 2A). Two pGolemi variants, P7A and F19A, reproducibly showed ill-behaved tryptophan perturbation profiles and were not included in further analysis. None of the pGolemi variants bound Mena$_{1-112}$ with higher affinity than did pGolemi (Table 1; Figure 2A), although several showed altered paralog specificity (vide infra).

Role of Residues Derived from ActA$_{11}$. First we consider pGolemi variants containing alanine in place of a residue derived from the *L. monocytogenes* protein ActA, namely, F2A, P3A, P6A, E9A, and E10A. These residues are located in the N-terminal half of pGolemi. Of the five, the lowest affinity is seen with F2A (K_d = 55 ± 6 μM); its complex with Mena$_{1-112}$ is 2.7 kcal·mol^{-1} less stable than the complex with pGolemi. P6A also binds Mena$_{1-112}$ poorly (K_d = 9 ± 2 μM), a 1.6 kcal·mol^{-1} loss relative to pGolemi. The remaining alanine variants, P3A, E9A, and E10A, as well as the sarcosine variants P3Z and P4Z, bind Mena$_{1-112}$ with affinities that are comparable to that of pGolemi. Interestingly, a pGolemi variant containing an additional ActA-

Table 1: Dissociation Constants of Complexes between pGolemi Variants and Peptides and $Mena_{1-112}$, $VASP_{1-115}$, or EVL_{1-115} at 25 °C[a]

	$K_{d\ Mena}$ (μM)	ΔG_{Mena} (kcal mol^{-1})	$K_{d\ VASP}$ (μM)	ΔG_{VASP} (kcal mol^{-1})	$\Delta\Delta G_{sp\ Mena\text{-}VASP}$ (kcal mol^{-1})	$K_{d\ Evl}$ (μM)	ΔG_{Evl} (kcal mol^{-1})	$\Delta\Delta G_{sp\ Mena\text{-}Evl}$ (kcal mol^{-1})	MRE_{222} (deg cm^2 dmol^{-1})
$ActA_{11}$	6 ± 2	-7	15 ± 4	- 6.6	-0.5	4.1 ± 0.3	-7.3	0.23	N.D.
pGolemi	0.6 ± 0.2	- 8.5	13 ± 2	- 6.7	-1.8	>100	> -5.5	< - 3.1	-16262
pGol-2	>100	> -5.5	15 ± 5	- 6.6	<1.1	10± 2	-6.8	< 1.3	-20386
P1A	0.8 ± 0.3	-8.3	5.4 ± 0.1	- 7.2	-1.1	20 ± 2	-6.4	-1.9	-5522
$P1A_{11}$	> 480	> - 4.5	>240	> - 5.3	N.C.	>240	> -4.9	N.C.	N.D.
F2A	55 ± 6	- 5.8	56 ± 3	- 5.8	0.0	106 ± 10	-5.4	-0.4	-13745
F2L	1.0 ± 0.1	-8.2	8.0 ± 0.4	- 6.9	-1.3	23 ± 1	-6.3	-1.9	-15052
P3A	2.3 ± 0.5	-7.7	[>75]	[> - 5.6]	N.C.	[> 50]	[> -5.9]	N.C.	-10745
P3Z	2.5 ± 0.3	-7.6	7 ± 1	- 7.0	- 0.6	> 50	> -5.9	< - 1.8	-9384
P4A	3.3 ±0.4	-7.5	4 ± 1	- 7.3	- 0.2	43 ± 5	- 6.0	-1.5	-8205
P4Z	2.4 ± 0.4	-7.7	5 ± 1	- 7.2	- 0.5	> 50	> - 5.9	< - 1.8	-5384
T5A	2.2 ± 0.2	-7.7	1.3 ± 0.2	- 8.0	0.3	13 ± 2	- 6.7	- 1.0	-8667
$T5A_{11}$	> 800	> - 4.2	> 240	> - 5.3	N.C.	210 ± 30	- 5.0	> 0.78	N.D
T5L	1.5 ± 1	- 7.9	10 ± 1	- 6.8	- 1.1	22 ± 1	- 6.4	- 1.5	-14647
P6A	9 ± 2	- 6.9	34 ± 3	- 6.1	- 0.8	[> 50]	[> - 5.9]	N.C.	-5937
P7A	[> 50]	[> - 5.9]	[> 100]	[> - 5.5]	N.C.	[> 100]	[> - 5.5]	N.C.	-2932
E9A	0.9 ± 0.2	- 8.2	8 ± 1	- 6.9	- 1.3	36 ± 3	- 6.1	- 2.2	-13115
E10A	1.2 ± 0.2	- 8.1	2.3 ± 0.3	- 7.7	- 0.4	32 ± 2	- 6.1	- 1.9	-8261
A11L	12 ± 2	- 6.7	8 ± 4	- 6.9	0.2	23 ± 10	- 6.3	- 0.4	- 12893
L16A	14 ± 3	- 6.6	> 50	> - 5.9	< - 0.7	>50	> - 5.9	< -0.7	-6714
F19A	[> 100]	[> - 5.5]	[> 100]	[> - 5.5]	N.C.	[>50]	[> - 5.9]	N.C.	-5756
L23A	77 ± 8	-5.6	> 50	> - 5.9	< 0.3	>50	> - 5.9	< 0.3	-4945
Y26A	3.0 ± 0.3	-7.5	> 50	> - 5.9	< - 1.7	>150	> - 5.9	< - 2.3	-7234
V29A	2.6 ± 0.5	-7.6	[> 50]	[> - 5.9]	N.C.	[>100]	[> - 5.9]	N.C.	-11797

[a] Also shown is the mean residue ellipticity at 222 nm of each variant in the absence of EVH1 domain (10 mM NaH_2PO_4 100 mM NaCl (pH 7.5) at 25 °C). Colors identify the location of alanine substitution: red and pink identify variants with substitution of an ActA-derived residue, whereas light blue and dark blue identify variants with substitution of an aPP-derived folding residue. Values in brackets indicate K_d values estimated from ill-behaved binding isotherms. N.D., not determined; N.C., not calculated. Two pGolemi variants, P7A and F19A, reproducibly showed ill-behaved tryptophan perturbation profiles, perhaps due to aggregation, and were not included in further analysis.

derived leucine in place of Ala11 (A11L) was a poor ligand for $Mena_{1-112}$ ($K_d = 12 \pm 2\ \mu M$, $\Delta\Delta G_{Mena} = 1.8$ kcal·mol^{-1}).

Role of Residues Derived from aPP. Next, we consider those eight variants (P1A, P4A, F7A, F19A, L16A, L23A, Y26A, and V29A) in which alanine is substituted for a residue that likely contributes to formation of the pGolemi hydrophobic core based on the crystal structure of aPP. This structure shows a core composed of side chains from residues at positions 5, 7, and 8 on the aPP PPII helix and residues 17, 20, and 24 on the α-helix; these positions correspond to residues 4, 6, 7, 16, 19, and 23 on pGolemi (Figure 1). These eight variants displayed widely varying affinities for $Mena_{1-112}$. Variants P1A, P4A, and Y26A formed complexes with $Mena_{1-112}$; the stabilities ($0.8\ \mu M \leq K_d \leq 3.3\ \mu M$) of these complexes were virtually identical to that of the corresponding pGolemi complex. Variants L16A and V29A, however, formed complexes having stabilities that were moderately destabilized ($14\ \mu M \leq K_d \leq 29\ \mu M$), and variants L7A, L19A, and L23A formed complexes having stabilities that could only be estimated ($K_d \geq 50\ \mu M$). In summary, substitution of ActA-derived residues of pGolemi located within the aPP PPII helix (Phe2, Pro3, and Pro6) significantly disrupts binding to $Mena_{1-112}$, whereas altering residues in the β-turn region (Glu9 and Glu10) does not. In general, substitutions of aPP-derived folding residues decrease binding if they are located in the center of the hydrophobic core, whereas those located near the termini do not. Overall, the affinity of variants for the $Mena_{1-112}$ domain ranged from 0.8 to ≥77 μM (ΔG_{Mena}, from −8.3 to ≥ −5.6 kcal·mol^{-1}), and $\Delta\Delta G_{Mena}$ ranged from 0.2 to 3.1 kcal·mol^{-1}. In a previous study of p007 (an aPP-based miniature protein generated through a combination of design and evolution), affinity of the alanine variants for specific hsCRE DNA ranged over $1.5 \leq K_d \leq 692$ nM ($\Delta G_{hsCRE} = -12$ to -8.4 kcal·mol^{-1}) (*54*). It is notable that despite having dramatically different targets, variants of both miniature proteins cover a similar range of binding energy differences.

Analysis of VASP Binding by pGolemi Variants. The affinity of each pGolemi variant for the EVH1 domain of VASP ($VASP_{1-115}$) was also determined using tryptophan perturbation analysis, as described above for $Mena_{1-112}$

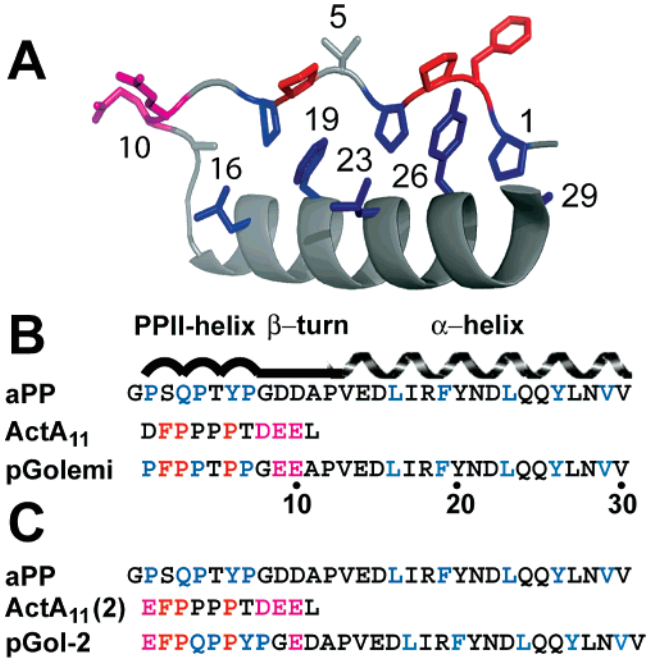

FIGURE 1: pGolemi variants and controls studied in this work. (A) Model of pGolemi structure obtained by substituting residues on aPP (PDB code: 1ppt). Shown in lines are the side chains of the residues that were changed to produce variant molecules. Residues in blue contribute to the aPP hydrophobic core, whereas those in red or magenta are derived from the sequence of $ActA_{11}$. The image was rendered in PyMol (Delano Scientific). (B) Sequence alignment of aPP and $ActA_{11}$ (proline-rich repeat 1, residues 264−274) used to design pGolemi (*65*). A schematic representation of the aPP secondary structure is shown above the corresponding primary sequence. Color coding is as described in (A). (C) Sequence alignment of aPP and $ActA_{11}$ (proline-rich repeat 2, residues 299−309) used to design pGolemi-2.

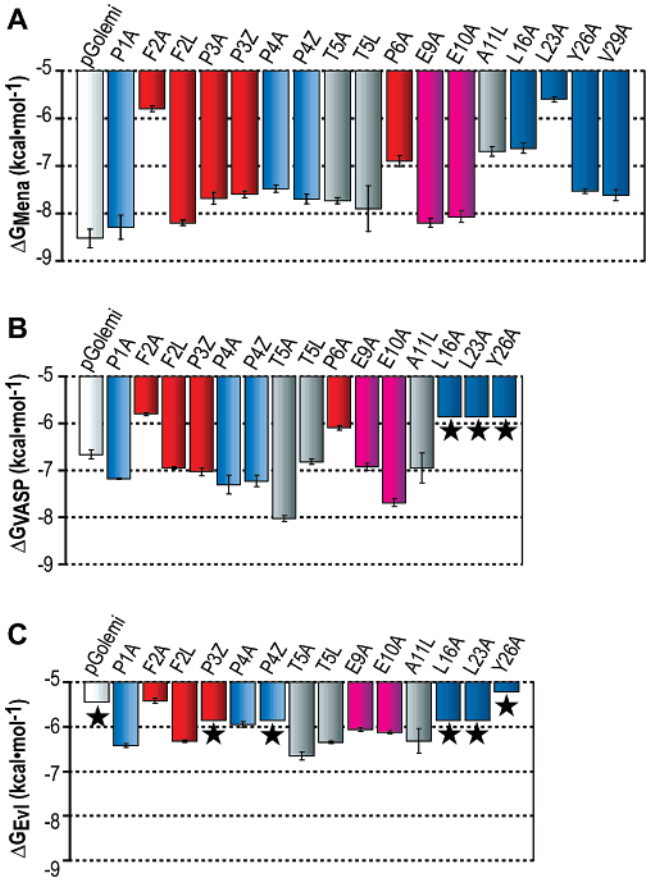

FIGURE 2: Histogram representing the relative affinities of pGolemi variants for (A) $Mena_{1-112}$, (B) $VASP_{1-115}$, or (C) Evl_{1-115}. Colors are described in Figure 1. Values of free energy were calculated from the relationship $\Delta G = -RT \ln K_d$. Stars denote complexes having affinities that could only be estimated. We note that in the case of two pGolemi variants, P7A and F19A, the increase in EVH1 domain fluorescence expected with increasing ligand did not resemble the expected sigmoidal curve, possibly due to ligand aggregation.

(Table 1; Figure 2B). Four variants (P3A, P7A, F19A, and V29A) reproducibly showed ill-behaved binding to $VASP_{1-115}$ and were not included in the analysis. Ten of the remaining variants bound $VASP_{1-115}$ as well as or better than pGolemi ($K_d = 13 \pm 2$ μM) with affinities ranging from 1.3 to 10 μM (Figure 2B). The highest $VASP_{1-115}$ affinity was observed with variant T5A ($K_d = 1.3 \pm 0.2$; $\Delta G = -8.0$ kcal·mol^{-1}). Substitution of leucine at position 5, in contrast, gives a variant with the same affinity for $VASP_{1-115}$ as pGolemi, within error, indicating that the residue identity at that position is important for $VASP_{1-115}$ affinity. Of the substitutions that lead to decreased $VASP_{1-115}$ affinity, two are for ActA-derived residues of pGolemi (F2A and P6A) and three are for aPP-derived folding residues in the α-helix (L16A, L23A, and Y26A). For the three α-helix residues, only an upper limit was reported because the upper plateau of the binding curve is not reached.

Analysis of Evl Binding by pGolemi Variants. The affinity of pGolemi variants for the EVH1 domain of Evl (Evl_{1-115}) was also measured by tryptophan perturbation, as described above for $Mena_{1-112}$ (Table 1; Figure 2B). Five variants showed ill-behaved binding to Evl_{1-115} and were not included in the analysis (P3A, P6A, P7A, F19A, and V29A). Although pGolemi does not detectably bind to Evl_{1-115} up to 100 μM ($\Delta G_{Mena} > -5.5$ kcal·mol^{-1}), eight variants with single amino acid substitutions show moderate affinity for this domain (Figure 2C), ranging from 13 to 43 μM ($\Delta G_{Mena} = -6.7$ to -6.0 kcal·mol^{-1}). The variant with the highest affinity for Evl_{1-115} is T5A ($K_d = 13 \pm 2$ μM; $\Delta G = -6.7$ kcal·mol^{-1}). The corresponding leucine variant, T5L ($K_d = 22 \pm 1$ μM; $\Delta G = -6.4$ kcal·mol^{-1}), has lower affinity. This sensitivity to minor perturbations reveals a subtle role for this position on Evl_{1-115} affinity. Other variants that bind Evl_{1-115} in the 20−50 μM range include P1A and P4A (substitution of aPP-derived folding residues in the PPII helix); F2L, E9A, and E10A (ActA-derived residues); and A11L (aPP-derived nonfolding residue). Of the variants that display low affinity for Evl_{1-115} by tryptophan perturbation ($K_d > 50$ μM), two have substitutions within ActA-derived residues (F2A and P3Z) and three have changes in aPP-derived folding residues (P4Z in the PPII helix; L16A, L23A, and Y26 A in the α-helix).

Analysis of Paralog Specificity: Mena versus VASP. The relative affinity of each variant for Mena and $VASP_{1-115}$ was compared to gain insight into the relative contribution, direct or indirect, of each amino acid substitution to the overall paralog specificity of pGolemi. The variant having a specificity profile that most closely resembles that of pGolemi ($\Delta\Delta G_{SP\ Mena-VASP} = -1.8$ kcal·mol^{-1}) is Y26A ($\Delta\Delta G_{SP\ Mena-VASP} < -1.7$ kcal·mol^{-1}). Other variants exhibiting similar selectivity include P1A ($\Delta\Delta G_{SP\ Mena-VASP} = -1.1$ kcal·mol^{-1}), E9A ($\Delta\Delta G_{SP\ Mena-VASP} = -1.3$ kcal·mol^{-1}), F2L ($\Delta\Delta G_{SP\ Mena-VASP} = -1.3$ kcal·mol^{-1}), and T5L

($\Delta\Delta G_{SP\ Mena-VASP} = -1.1$ kcal·mol^{-1}). The data suggest that the residues substituted in these cases do not contribute significantly to paralog specificity.

pGolemi variants having specificity profiles that differ from that of pGolemi fall into three categories. First, decreased affinity for both $Mena_{1-112}$ and $VASP_{1-115}$ ($K_d >$ 50 μM) is seen for two variants, F2A ($\Delta\Delta G_{SP\ Mena-VASP} = 0$ kcal·mol^{-1}) and L23A ($\Delta\Delta G_{SP\ Mena-VASP} < 0.3$ kcal·mol^{-1}). This paralog-independent reduction in specificity, resulting from changes in both a presumed direct binding residue (Phe2) and a folding residue (Leu 23), emphasizes the role miniature protein fold in controlling the fidelity of EVH1 domain interactions.

Paralog-dependent differences in affinity arising from an increase in affinity for $VASP_{1-115}$ that may be coupled with decreased affinity for $Mena_{1-112}$ are seen in a second category of variants. The most striking examples are T5A and A11L, which have specificity profiles that are the reverse of pGolemi's ($\Delta\Delta G_{SP\ Mena-VASP}$ of 0.3 and 0.2 kcal·mol^{-1}, respectively). We note that both T5A and A11L are altered at aPP-derived nonfolding residues. Two other variants that show less dramatic effects are P3Z ($\Delta\Delta G_{SP\ Mena-VASP} = -0.6$ kcal·mol^{-1}) and E10A ($\Delta\Delta G_{SP\ Mena-VASP} = -0.4$ kcal·mol^{-1}), which have substitutions at ActA-derived residues. In contrast, modestly reduced affinity for both $Mena_{1-112}$ and $VASP_{1-115}$ is the hallmark of a third category of variants. For example, variants P6A and L16A both show moderate affinity for $Mena_{1-112}$ ($K_{d\ Mena} = 9 \pm 2$ and 14 ± 3 μM, respectively), whereas $VASP_{1-115}$ affinity is decreased ($K_{d\ VASP} = 34 \pm 3$ and >50 μM, respectively). The resultant specificity phenotype is therefore similar to but less pronounced than that of pGolemi ($\Delta\Delta G_{SP\ Mena-VASP} = -0.8$ kcal·mol^{-1} for P6A and <-0.7 kcal·mol^{-1} for L16A). The data suggest that the residue identities at positions 3, 5, 10, and 11 contribute to paralog specificity primarily by modulating affinity for $VASP_{1-115}$, whereas those at positions 6 and 16 affect affinity for both $Mena_{1-112}$ and $VASP_{1-115}$.

Analysis of Paralog Specificity: Mena versus Evl. The same approach was taken to evaluate the relative roles of each amino acid substitution in determining specificity between $Mena_{1-112}$ and Evl_{1-115}. Several variants recapitulate the pGolemi specificity profile (i.e., $K_{d\ Mena} < K_{d\ Evl}$), including P3Z ($\Delta\Delta G_{SP\ Mena-Evl} < -1.8$ kcal·mol^{-1}), P4Z ($\Delta\Delta G_{SP\ Mena-Evl} < -1.8$ kcal·mol^{-1}), and Y26A ($\Delta\Delta G_{SP\ Mena-Evl} < -2.3$ kcal·mol^{-1}), but none show the same dramatic difference in affinity between $Mena_{1-112}$ and Evl_{1-115} as pGolemi ($\Delta\Delta G_{SP\ Mena-Evl} < -3.1$ kcal·mol^{-1}). This observation suggests that these three residue positions are not implicated in Mena-Evl specificity. As was seen in the Mena-VASP analysis, substitution of Phe2 or Leu23 for Ala decreases Mena-Evl specificity by a paralog-independent mechanism in that affinity is >50 μM for both domains. This result further underscores the importance of the residue identity at these positions in establishing basal EVH1 affinity. Variants with substitutions for other residues also maintain the general specificity profile of pGolemi but exhibit a range of intensities. An increase in affinity for Evl_{1-115} accompanied by little or no difference in $Mena_{1-112}$ affinity is seen in variants with substitutions for ActA-derived residues (F2L, $\Delta\Delta G_{SP\ Mena-Evl} = -1.9$ kcal·mol^{-1}; E9A, $\Delta\Delta G_{SP\ Mena-Evl} = -2.2$ kcal·mol^{-1}; E10A: $\Delta\Delta G_{SP\ Mena-Evl} = -1.9$ kcal·mol^{-1}), as well as for an aPP-derived PPII-helix folding residues (P1A, $\Delta\Delta G_{SP\ Mena-Evl} = -1.9$ kcal·mol^{-1}; P4A, $\Delta\Delta G_{SP\ Mena-Evl} < -1.5$ kcal·mol^{-1}) and a nonfolding residue (T5A, $\Delta\Delta G_{SP\ Mena-Evl} = -1.0$ kcal·mol^{-1}; T5L, $\Delta\Delta G_{SP\ Mena-Evl} = -1.5$ kcal·mol^{-1}). Reduced specificity is also observed upon substitution of an aPP-derived α-helix folding residue, L16A ($\Delta\Delta G_{SP\ Mena-Evl} < -0.7$ kcal·mol^{-1}), resulting from decreased $Mena_{1-112}$ affinity. In contrast, the loss of specificity of a variant in which an aPP-derived nonfolding residue is changed, A11L ($\Delta\Delta G_{SP\ Mena-Evl} = -0.4$ kcal·mol^{-1}), is the result of a concurrent increase in Evl_{1-115} affinity ($K_d = 23 \pm 10$ μM) and a decrease in Mena affinity ($K_d = 12 \pm 2$ μM). To summarize, the data suggest that the identity of residues throughout pGolemi affect Mena-Evl specificity primarily through modulation of Evl affinity (F2L, E9A, E10A, P1A, and T5A), Mena affinity (L16A), or both (A11L).

Alternate Designed EVH1 Domain-Specific Miniature Protein: pGol-2. We also explored an alternative design, pGol-2, that differs from pGolemi in terms of how the sequences of $ActA_{11}$ and aPP are aligned and by the addition of a glutamate residue at the N terminus that has been shown to improve the affinity of peptide ligands for EVH1 domains (*46*) (Figure 1B). Interestingly, pGol-2 shows the reverse specificity profile of pGolemi (Table 1): no binding to $Mena_{1-112}$ is detected at concentrations as high as 100 μM, whereas the $VASP_{1-115}$ affinity is comparable to that of pGolemi. Moreover, the affinity of pGol-2 for Evl_{1-115} is higher than that for any of the pGolemi variants ($K_d = 10 \pm 2$ μM).

Secondary and Tertiary Structures of pGolemi Variants. The α-helical content of each pGolemi variant was measured by circular dichroism (CD) spectroscopy, and the mean residue ellipticities at 222 nm (MRE_{222}) for each are reported in Table 1. In general, variants that retain significant α-helical character at 25 °C also melt cooperatively. With the exception of variant E9A ($T_m = 54$ °C), none of the variants are better folded than pGolemi ($T_m = 42$ °C). As expected, substitution of aPP-derived folding residues in variants P1A, P4A, P7A, L16A, F19A, L23A, and Y26A leads to a dramatic decrease in α-helix secondary structure. pGol-2 is also well folded, with a greater α-helix content ($MRE_{222} = -20386$ deg·cm^2 dmol^{-1}) and a higher melting temperature ($T_m = 50$ °C) than pGolemi.

Effect of pGolemi Variants on L. monocytogenes Motility. The bacterium *L. monocytogenes* achieves motility by recruiting Ena/VASP proteins through a direct interaction with the *L. monocytogenes* cell surface protein ActA. A cell-free assay for *L. monocytogenes* motility in *X. laevis* oocyte extract has provided a valuable model system for studying mechanisms of actin cytoskeleton (*66*, *68*). In previous work, we reported that the presence of 10−27 μM pGolemi decreased the speed of *L. monocytogenes* motion in *X. laevis* oocyte extract (*65*) by 68%, consistent with the work of others in which the EVH1 binding motifs were removed from ActA (*70*−*73*) or when Ena/VASP proteins were removed from cell extracts (*74*). Additionally, pGolemi caused extreme speed variation and the formation of discontinuous actin comet tails. In contrast, the addition of a nonspecific EVH1 domain ligand, an 11-residue peptide derived from the proline repeat region of ActA, at the same concentration results in a speed reduction of 85% (*65*, *69*) with no observed speed variation. We hypothesized that the discontinuous tails

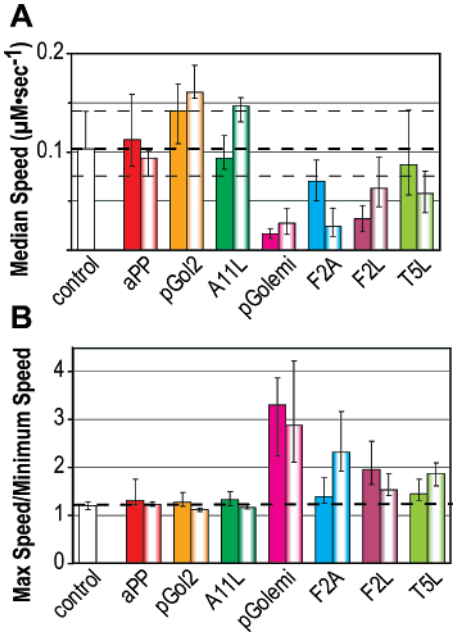

FIGURE 3: (A) Plot of median speed (μm·s^{-1}) of *L. monocytogenes* in the absence (white) or presence of the indicated ligand at 10 μM (dark) and 100 μM (light). Error bars represent the 25th (−) and 75th (+) percentiles of moving bacteria. The numbers of bacteria analyzed at 10 and 100 μM, respectively, for each miniature protein were 46 and 9 (aPP), 39 and 7 (pGol2), 33 and 21 (A11L), 15 and 27 (pGolemi), 62 and 41 (F2A), 38 and 28 (F2L), 59 and 23 (T5L), and 68 (control in the absence of miniature protein).

might result from the high paralog specificity observed in vitro. To test this hypothesis, a selection of miniature proteins showing a range of affinities toward the EVH1 domains of $Mena_{1-112}$, $VASP_{1-115}$, and Evl_{1-115} were analyzed for their effects on *L. monocytogenes* median speed and speed variability (maximum/median speed ratio) (Figure 3). Under control conditions (aPP_{1-31}, or no miniature protein ligand), the median bacterial speeds is 0.10 ± 0.03 μm s^{-1}, which is comparable to literature reports of 0.10 ± 0.01 μm s^{-1} (*68*), and the speed variability ratio is 1.20 ± 0.08. In the presence of 10 μM pGolemi, the median speed is reduced by 83%, as reported previously (0.017 ± 0.005, n = 46) (*66*), and the speed variability ratio was higher than that of all tested miniature proteins (3.3 ± 0.8). At 10 μM, only variant F2L showed a significant reduction in median speed (69%; 0.03 ± 0.01 μm s^{-1}, n = 62) and an increase in speed variability (2.0 ± 0.4) (Figure 3A). Surprisingly, pGol-2 at 10 μM caused a significant (p < 0.01) increase in median speed of 38% (0.14 ± 0.03 μm s^{-1}, n = 39); however, speed variability was similar to that of the control. At 100 μM, pGolemi, F2A, and T5L showed a significant (p < 0.01) decrease in median speed (pGolemi, 0.03 ± 0.01 μm s^{-1}, n = 27; F2A, 0.02 ± 0.01 μm s^{-1}, n = 41; T5L, 0.06 ± 0.02 μm s^{-1}, n = 23) accompanied by an increase in speed variability (pGolemi, 3 ± 1; F2A, 2.3 ± 0.6; T5L, 1.9 ± 0.2). F2L caused a decrease in speed (0.06 ± 0.02 μm s^{-1}, n = 28), but speed variability was comparable to that of the control. In contrast, A11L and pGol-2 both caused significant (p < 0.05) increases in median speed compared to controls at this concentration (A11L, 0.15 ± 0.02 μm s^{-1}, n = 21; pGol-2, 0.160 ± 0.006 μm s^{-1}, n = 7), with speed variability comparable to that of the control.

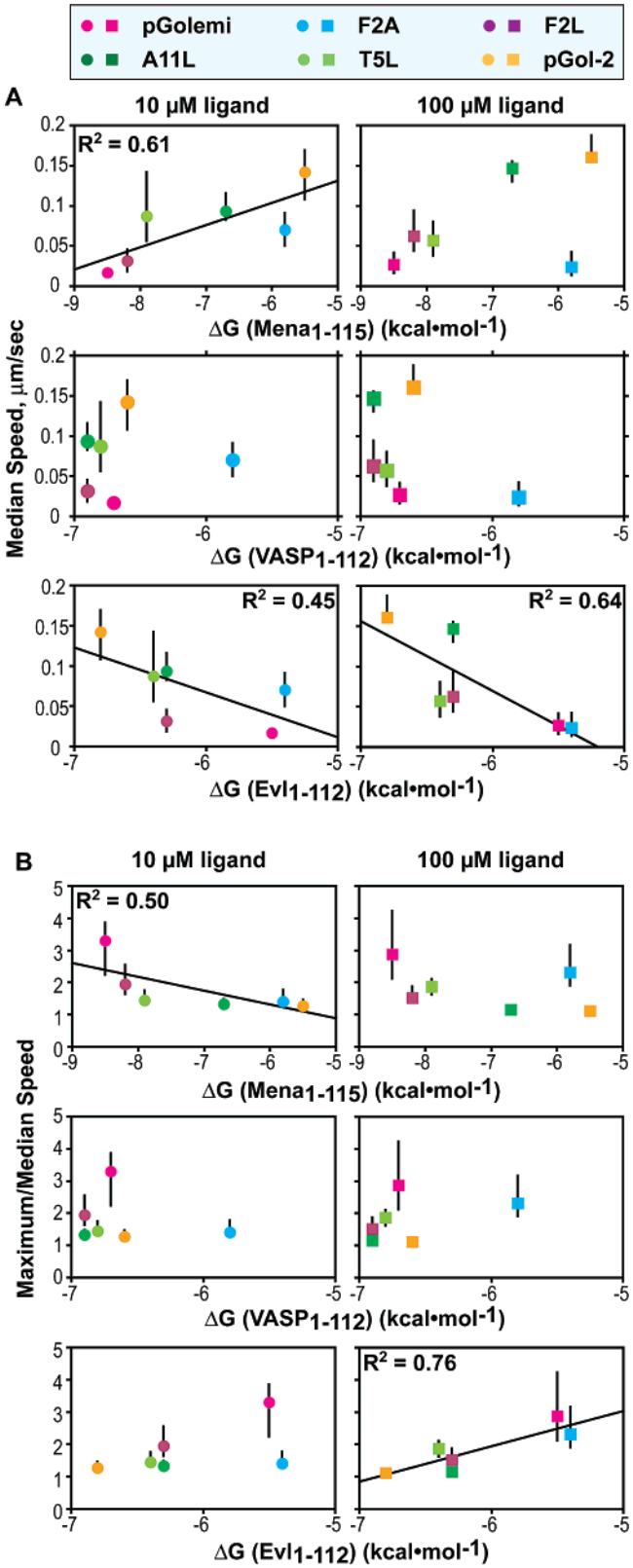

FIGURE 4: Quantitative analysis of *L. monocytogenes* motility as a function of EVH1 domain affinity. Plots of (A) median speed and (B) the ratio of the maximum to median speed in the presence of 10 or 100 μM miniature protein are shown as a function of EVH1 domain affinity. Error bars represent the 25th (−) and 75th (+) percentiles of moving bacteria.

Plotting speed or speed variability against EVH1 domain affinity for these selected miniature proteins reveals unexpected trends (Figure 4). Increased affinity for $Mena_{1-112}$

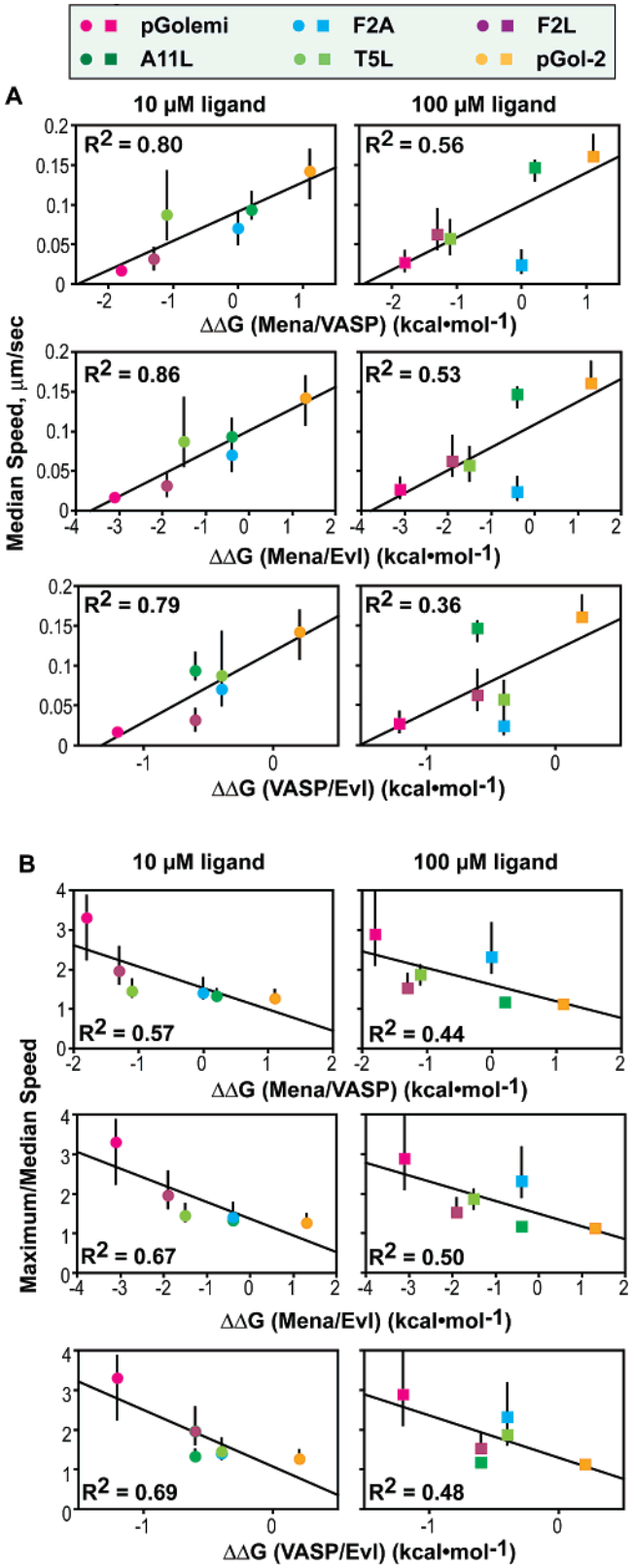

FIGURE 5: Quantitative analysis of *L. monocytogenes* motility as a function of EVH1 domain specificity. Plots of (A) median speed and (B) the ratio of the maximum to median speed in the presence of 10 or 100 μM miniature protein are shown as a function of EVH1 domain specificity. Error bars represent the 25th (−) and 75th (+) percentiles of moving bacteria.

correlates weakly with decreased speed and increased speed variability of motile bacteria in the presence of miniature protein, whereas the reverse trends are observed for Evl_{1-115} affinity. There is no obvious relationship between $VASP_{1-115}$ affinity and the motility of *L. monocytogenes* in these assays. The median speed and maximum/median speed ratios were also plotted against the EVH1 domain specificity of each miniature protein or variant for pairs of EVH1 domain paralogs to identify relationships between specificity and aberrant *L. monocytogenes* motility (Figure 5). A strong linear correlation was observed for both metrics at 10 μM miniature protein, indicating that high specificity, particularly modest binding to $VASP_{1-115}$ and especially Evl_{1-115}, is related to decreased speed and increased speed variability. These observations hold but are less striking for assays conducted using 100 μM ligand.

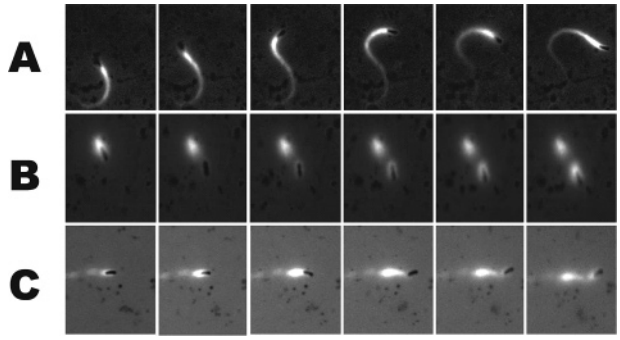

FIGURE 6: Time-lapsed images of *L. monocytogenes* motility visualized using (A, B) rhodamine-labeled phalloidin to visualize the actin cytoskeleton or (C) $pGolemi^{Flu}$. Time-lapsed images were taken at 25 s intervals under fluorescence illumination. (A) In the absence of pGolemi, *L. monocytogenes* (black rods) moves rapidly at steady state. (B) In the presence of 27 μM pGolemi, *L. monocytogenes* moves slowly and actin tails are discontinuous. (C) $pGolemi^{Flu}$ (white) at 27 μM is integrated into the actin tail in a discontinuous pattern.

pGolemi Localizes to the Actin Tail−Bacterium Interface. A fluorescently tagged analogue of pGolemi was used to monitor localization under the conditions of the *L. monocytogenes* motility assay. At a concentration of 27 μM, $pGolemi^{Flu}$ appeared as a short, bright tail attached to the *L. monocytogenes* cell surface (Figure 6) that elongated as the bacterium accelerated forward. The observation that pGolemi, a ligand for the EVH1 domain of Mena, localizes to the actin surface at the interface between the bacterium and the comet tail is in agreement with previous studies that show that Ena/VASP proteins are localized at the distal pole of motile *L. monocytogenes* (*11*, *75*, *76*, *77*). Ena/VASPs act as indirect links by attaching to the proline-rich repeat region of the bacterial surface protein ActA through their EVH1 domain (*75*, *76*) and also to actin filaments through the EVH2 domain (*74*). The tail can also attach directly to the bacterium by binding sites on ActA. The observation of the discontinuous tails in the presence of a specific inhibitor of EVH1 domain interactions suggests a weakening of the Ena/VASP-mediated molecular connections between the tail and the bacterium.

DISCUSSION

pGolemi Contains an aPP-like Fold and Binds the Mena EVH1 Domain in a Manner analogous to $ActA_{11}$. Structural (*42*), biochemical (*72*, *78*), and functional (*79*, *80*) studies of Ena/VASP proteins have highlighted the critical importance of the aromatic residue of EVH1 domain ligands, which contributes to affinity through shape complementarity to the V-shaped pocket within the binding surface and by setting

the correct register and orientation of the PPII helix (*42*), reviewed in *39*. For unstructured peptide ligands, the aromatic residue can be substituted for any aromatic residue or leucine with little or no loss in affinity (*46*, *71*, *80*, *82*). pGolemi shows analogous behavior: the variant containing alanine in place of phenylalanine at position 2 (F2A) exhibits a dramatic loss in affinity for $Mena_{1-112}$, whereas the corresponding leucine variant (F2L) does not. Maintenance of the type II polyproline helix conformation is also important for EVH1 domain binding, but as with short ActA-derived peptides (*71*), single amino acid substitutions at residues Pro3, Pro4, and Pro6 lead only to small reductions in $Mena_{1-112}$ affinity, indicating that the secondary structure is not significantly perturbed.

Structural data from CD and AU are consistent with a model in which monomeric pGolemi adopts an aPP-like fold in the absence of the EVH1 domain. Substitution of alanine at pGolemi residue positions that are important for aPP folding (in variants P1A, P4A, P7A, L16A, F19A, L23A, Y26A, and, to a lesser extent, V29A) leads to significant decreases in the MRE_{222} signal by CD, consistent with previous studies on DNA-binding miniature proteins (*54*). We note that the structure of pGolemi is also sensitive to the identity of amino acids substituted for Thr5, a position not previously identified as critical for miniature protein folding. This observation suggests that the ActA residues grafted onto the aPP scaffold have resulted in differences in the packing of the miniature protein's hydrophobic core, which likely results in altered presentation of surface residues as well. Any effect the substitutions have on the aggregation state is not known.

Residues throughout the pGolemi Sequence Contribute to EVH1 Domain Affinity. Every pGolemi variant except P1A, T5L, and E9A exhibited decreased affinity for $Mena_{1-112}$. Among variants containing alanine in place of a residue derived from ActA, significant loss of binding was observed only upon alteration of Phe2, the key aromatic residue from the binding epitope, and Pro6, which is located centrally within the pGolemi sequence. Substitution of the remaining ActA-derived residues resulted in only minor losses in binding energy, consistent with the observations of others, suggesting that these residues serve a scaffolding role to maintain the epitope's secondary structure (*42*, *45*, *72*). Analysis of the effects of altering aPP α-helix-derived residues shows that three residues located centrally in the primary sequence, Ala11, Leu16, and Leu23, are important for binding. Leucine substitution for Ala11 does not significantly perturb α-helix structure, but alanine substitution for either Leu16 and Leu23 causes a dramatic loss in α-helical secondary structure, consistent with the role of these positions in packing the hydrophobic core of an aPP-like scaffold in this and other miniature proteins (*54*). In contrast, variants with substitutions for aPP-derived folding residues located near the termini of the pGolemi sequence, Pro1, Tyr26, and Val29, suffer small or negligible reductions in $Mena_{1-112}$ binding despite the fact that they are relatively unstructured. Taken together with the observation that truncated peptides containing only the PPII helix portion do not bind to $Mena_{1-112}$ (this work; *65*), these data support the notion that the C-terminal portion of the pGolemi sequence is critical to $Mena_{1-112}$ affinity. The data leave open to question whether Ala11, Leu16, and Leu23 contribute to binding by direct contact or indirect conformational effects; however, additional data could provide the necessary insight into the separate or combined functions of these residues. In general, residue substitutions that most significantly diminished $Mena_{1-112}$ also decreased the already moderate affinity for $VASP_{1-115}$; any negative impact on Evl_{1-115} binding could not be evaluated because of the low affinity of the Evl_{1-115}·pGolemi complex. Variants with improved affinity for both $VASP_{1-115}$ and Evl_{1-115} bore substitutions for aPP-derived PPII helix folding residues (Pro1 and Pro4), aPP-derived nonfolding residues (Thr5 and Ala11), and ActA-derived residues (Glu9 and Glu10; Pro3 for $VASP_{1-115}$ only). Notably, F2L showed improved affinity for both $VASP_{1-115}$ and Evl_{1-115}. Short peptide fragments of ActA studied by Ball and co-workers (*46*) show the opposite trend in VASP EVH1 binding for Phe versus Leu at the equivalent position, highlighting a difference between miniature protein and unfolded peptide ligands. The observation that small changes can improve affinity for $VASP_{1-115}$ and Evl_{1-115} also points to the possibility of using phage display to evolve pGolemi into second generation miniature proteins with high affinity for these paralogs.

Residues throughout the pGolemi Sequence Contribute to EVH1 Paralog Specificity. Mutational analyses of ActA peptides and endogenous host cell Ena/VASP binding partners indicate that the EVH1 ligand is (D/E)(F/L/W/Y)-P$X\phi$PX_{1-3} (abbreviated FP4), where X is any amino acid and ϕ is hydrophobic (*71*). Short peptides containing this consensus bind EVH1 domain paralogs with similar affinities (*46*, *65*, *71*). Ball and co-workers compared the binding of the EVH1 domains of Mena and VASP for 6−13 residue ActA peptide variants by fluorescence perturbation and found that the interaction with $Mena_{1-112}$ was universally of higher affinity (*46*). Truncations at the termini as well as single amino acid substitutions decreased affinity for both $Mena_{1-112}$ and $VASP_{1-115}$. Niebuhr and co-workers used solid-phase binding studies to compare the relative binding of Mena and VASP to 10-residue peptide ligands (*71*) and found that within the core consensus, certain substitutions, particularly at position 2 but also positions 3, 4, and 6 (pGolemi numbering), could lead to selectivity between $Mena_{1-112}$ and $VASP_{1-115}$. The pGolemi variants in our study all showed the general trend of higher affinity for $Mena_{1-112}$ than for $VASP_{1-115}$ (or Evl_{1-115}), with the exception of A11L and T5A.

The effects of single amino acid changes in pGolemi on the striking EVH1 paralog binding specificity fall into two broad groups. Positions at which substitution results in significantly reduced binding to all three class I EVH1 domains include the key aromatic residue from the EVH1 binding epitope, Phe2, and the aPP-derived α-helix folding residues, Leu16 and Leu23. Substitutions at the remaining residue positions show a spectrum of paralog specificity profiles resulting from modulated affinity toward $Mena_{1-112}$, $VASP_{1-115}$, and Evl_{1-115}. In general, substitutions for ActA-derived residues (F2L, P3A and P3Z, P6A, E9A, and E10A) had a mild negative effect on $Mena_{1-112}$ affinity and a positive effect on affinity for $VASP_{1-115}$ and Evl_{1-115}. P6A is an exception in that affinity is decreased for both $Mena_{1-112}$ and $VASP_{1-115}$ (the effect on Evl_{1-115} affinity is not known). One study of paralog-dependent effects of binding by short (10 residue) ActA-derived peptide variants showed that the

F2L substitution (pGolemi numbering), for example, diminished affinity for VASP (*71*). In another study of ActA peptoids containing N-substituted residues at the Pro3 position, species with long, hydrophobic side chains bound to VASP, but those with short side chains, such as sarcosine, did not (*72*). The epitope-derived residues are therefore important for determining paralog specificity, but sequence context is relevant. aPP-derived residues also play a role in paralog specificity. Substitutions for folding residues in the PPII helix portion of the molecule generally did not affect (P1A) or slightly decreased (P4A, P4Z) affinity for $Mena_{1-112}$, but conferred increased affinity for both $VASP_{1-115}$ and Evl_{1-115}. The global decrease in EVH1 affinity of variants with substitutions for two α-helix folding residues (L16A and L23A) exemplifies the paralog-independent role of these residues in specificity; on the other hand, the Y26A substitution resulted in an enhanced version of pGolemi's paralog specificity profile, with only a slight decrease in $Mena_{1-112}$ affinity but no detectable binding to either $VASP_{1-115}$ or Evl_{1-115} up to at least 50 μM. Two additional aPP-derived residues, Thr5 and Ala11, were also implicated as major determinants of paralog specificity by modulating affinity to all three domains by increasing affinity for both $VASP_{1-115}$ and Evl_{1-115} while slightly decreasing $Mena_{1-112}$ affinity. These data provide evidence that pGolemi residues outside the binding epitope have a spectrum of roles that subtly influence paralog specificity.

Overall, the analysis of pGolemi specificity provides a detailed map of the effects of residue substitutions on basal EVH1 domain affinity as well as paralog specificity. The importance of the context of epitope presentation (i.e., unfolded peptide vs miniature protein) in specificity is highlighted by the observation of sometimes contradictory effects of analogous substitutions across different studies of EVH1 domain−ligand interactions. This data collection will be invaluable in guiding the design of miniature protein libraries for the purpose of discovering molecules with desired interaction specificity profiles.

Limited Relationship between Mena, but Not VASP or Evl, Affinity and α-Helix Secondary Structure. Cocrystal structures of the EVH1 domains of Mena and Evl in complex with short ActA peptide ligands show that the peptide adopts a type II polyproline helix secondary structure conformation (*42*, *45*). α-Helical epitopes having restricted conformations because they are presented in the context of a miniature protein (*54*) pay a lower entropic cost upon binding to their cognate domains because they are prestructured. In contrast, short peptides (>10 residues) containing sequences with a propensity toward forming type II polyproline helices can spontaneously adopt this conformation in aqueous solution (*37*). Our initial report of pGolemi design, structure, and function showed that the portion of the molecule derived from the α-helix of aPP contributes at least 3.5 kcal·mol^{-1} to $Mena_{1-112}$ binding (*65*), raising the question of whether the α-helix plays an analogous role in prestructuring or whether some other mechanism is involved. We investigated the premise that the aPP fold contributes to binding by plotting the intensity of the α-helix signature (MRE_{222}) of the pGolemi variants against affinity for $Mena_{1-112}$, $VASP_{1-115}$, and Evl_{1-115} (Figure 7).

Examination of the data in Figure 7 suggests that, in general, pGolemi variants possessing high levels of α-helix secondary structure in the absence of bound EVH1 domain also possess the highest affinity for $Mena_{1-115}$ (Figure 7A). There are three clear outliers to this trend: F2A and A11L, which are well folded but bind $Mena_{1-115}$ with low affinity,

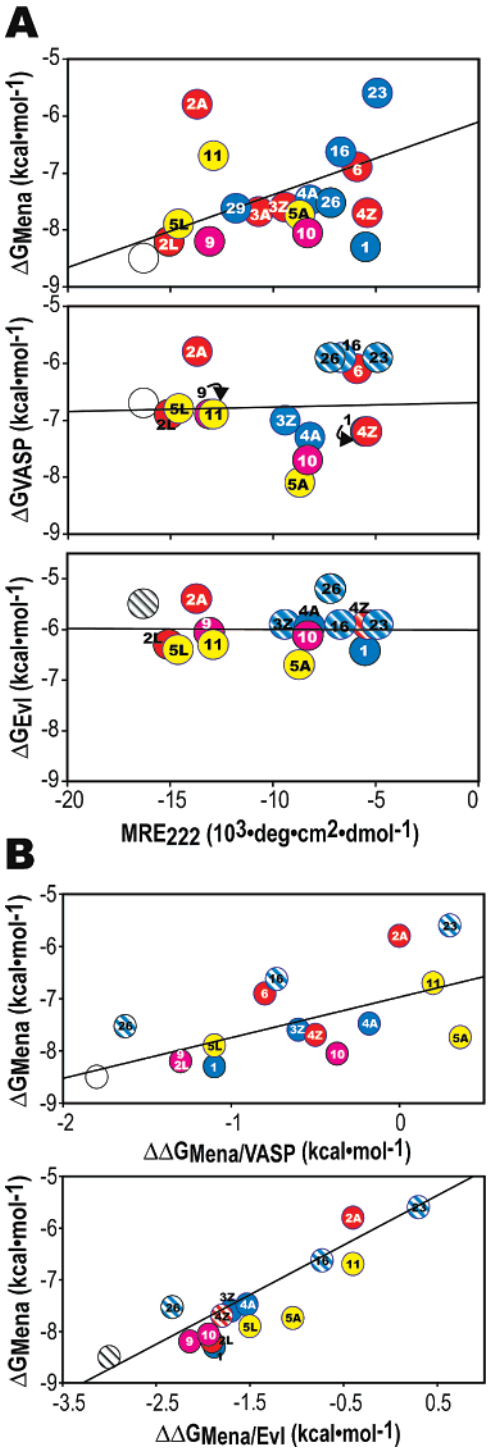

FIGURE 7: Relationship between (A) miniature protein secondary structure (MRE_{222}) and binding free energy of complexes with $Mena_{1-112}$, $VASP_{1-115}$, and Evl_{1-115}. (B) Relationship between the affinity of a miniature protein for $Mena_{1-112}$ or $VASP_{1-115}$ and either $Mena_{1-112}/VASP_{1-115}$ or $Mena_{1-112}/Evl_{1-115}$ specificity. Letters represent the amino acid substituted at the position shown. Variants containing substitutions derived from ActA are shown in red (FP4 core) or pink (flanking acidic residues). Variants containing substitutions derived from aPP are shown in blue. Other variants are in yellow. pGolemi is shown in white. Stripes represent variants for which only a lower limit of affinity was determined.

and P1A, which is poorly folded but binds $Mena_{1-115}$ well. If, as argued above, pGolemi and $ActA_{11}$ bind $Mena_{1-115}$ in a similar manner, then Phe2 is involved in direct contact with the domain, so low affinity of F2A results from disruption of a key epitope residue and not from loss of structure. In the case of Ala11, substitution for leucine does not reduce folding; however, changing the identity of the side chain at this position results in modulated affinity for all three paralogs (this work). It can therefore tentatively be concluded that Ala11 also contacts the domain surface. In the case of P1A, given that the 11-residue truncated version of this variant does not bind $Mena_{1-112}$, the likely role of this residue is primarily in maintaining the folded structure rather than in direct domain contact. Because $Mena_{1-112}$ binding is very sensitive to other substitutions that disrupt α-helix structure, it may be that this particular variant can fold upon binding with the energetic cost being paid by the increased availability of ligand conformations that are highly favorable to $Mena_{1-112}$ binding. Alternatively, P1A might remain unfolded even after binding, the high affinity arising from the fact that more of the hydrophobic area of the molecule is exposed, thus allowing nonspecific interactions to form following the initial recruitment effected by the FP4 core. Overall, the data support the claim that the presentation of the EVH1 domain binding epitope in the context of an aPP scaffold results in improved affinity for $Mena_{1-112}$ through stabilization of the tertiary structure, which in turn emerges from the synergistic interactions of the α- and PPII helices. In contrast to the positive trend between structure and $Mena_{1-112}$ binding, no such relationship exists for either $VASP_{1-115}$ or Evl_{1-115}. This suggests that, as was seen with in vitro evolution of p007 (*53*), maintaining or restoring structure will be an important consideration during future efforts to generate high-affinity miniature proteins for the other EVH1 paralogs. Plots of the α-helicity of pGolemi variants and their specificity reveal no correlation.

Direct Relationship between Affinity and Specificity. The data suggest that there exists a direct relationship between the affinity of a pGolemi variant for $Mena_{1-115}$ and its ability to discriminate $Mena_{1-112}$ from the other EVH1 paralogs (Figure 7). Such a relationship has also been observed for the miniature protein p007, which binds DNA with high affinity and specificity, as well as in a wide range of other systems, ranging from selective binding of Na^+ versus K^+ (*85*) to affinity-matured antibodies (*86*) to RNA aptamers (*87*). The laws of thermodynamics do not explicitly supply a connection between ΔG_{Mena} and ΔG_{Spec}; however, in all of these cases, the relationship has been rationalized on the basis of ligand preorganization. This relationship also leads to the conclusion that by presenting a naturally evolved epitope fragment that binds with relatively high affinity to a protein domain in the context of a well-folded scaffold, a new dimension of specificity can be added to the ligand's functional characteristics.

Aberrant Motility of Listeria Is Correlated with EVH1 Paralog Specificity. The use of peptides to perturb protein−protein interactions is an established approach that has been used to provide important insights into the mechanisms of cytoskeleton control, and the motility of *L. monocytogenes* in particular. In 1994, Southwick and co-workers reported that microinjecting an FP_4-containing peptide into PtK2 cells infected with *L. monocytogenes* blocked tail elongation and halted motility, but microinjection of poly-L-proline led to increased tail length and bacterial speed (*69*). Niebuhr and co-workers' engineered *L. monocytogenes* to lack the EVH1 domain binding site of ActA and demonstrated that the bacteria could still accumulate actin at their surfaces but at a reduced level (*71*). Actin was eventually able to polarize and form a stubby tail, which allowed motility to proceed at a dramatically reduced speed. Our observation that pGolemi binds EVH1 domains in a similar manner to ActA peptides and also causes a decrease in median speed of *L. monocytogenes* is therefore in agreement with the work of others in that EVH1−ActA interactions are required to maintain speed.

Discontinous actin tails have been observed in previous studies of *L. monocytogenes* motility at steady state using a variety of systems, including cell culture infection and cell extracts (*61*, *62*), as well as in the context of ActA-coated beads, where motility was reconstituted using purified proteins (*63*). The first example was described by Lasa et al. as a result of the deletion of residues 21−97 of ActA, the site of interaction with the actin branching and nucleating Arp2/3 complex (*61*). Lauer et al. observed this phenotype in an alanine scanning of the charged residues of the ActA protein in the region that spanned from 165 to 260, which is outside the polyproline-rich repeat region (63−390) (*62*). In *63*, discontinuous tails were seen when monitoring the motility of ActA-coated beads in a reconstituted motility medium lacking VASP in a reconstituted motility medium. Our results specifically implicate the EVH1−ActA interaction in this phenotype. More recently, a study of the process of initiation of *Listeria* motility showed that hopping is in fact a characteristic step in the transition between polarized actin cloud formation and the establishment of tails that can maintain persistent speed and direction (*64*). Actin accumulates at one of the poles and bacteria start to move forward with a sudden burst of speed that breaks the link with the tail. Bacteria come to a complete stop upon collision with a physical obstruction in the medium, and the process repeats until a long, weak tail develops that eventually matures into a robust tail capable of maintaining speed and directionality. In that study, disruption of the EVH1 binding site by mutating the key Phe in the binding epitope of ActA showed an effect similar to treatment of wild-type *L. monocytogenes* with pGolemi in that erratic hopping motility persisted and tails did not follow through the maturation process. In all of the cases of discontinuous tails, an imbalance between the propulsive and retarding forces is likely responsible for trapping the bacteria or bead in an intermediate stage of tail development. For the cases where Ena/VASP−ActA interactions are implicated, the imbalance may be due to bursts of propulsion by rapid actin polymerization, partially overwhelming the weakened molecular connection between the tail and the bacteria or bead. The clear correlation between the effect of pGolemi on *L. monocytogenes* motility and the miniature protein's in vitro properties as a paralog-specific inhibitor of protein−protein interactions taken together with the fact that hopping motility is a stage in the tail maturation process suggests that the different Ena/VASP paralogs may not play equivalent roles in the transition from the initiation phase to robust motility. Future work will explore this hypothesis further.

ACKNOWLEDGMENT

We thank James Lear and Abby Maranda for assistance with analytical ultracentrifugation and Julie Theriot for assistance with analyzing *L. monocytogenes* motility data.

SUPPORTING INFORMATION AVAILABLE

Procedures for protein expression, peptide synthesis and purification, K_d determination, CD, and motility analysis. This information is available free of charge via the Internet at http://pubs.acs.org.

REFERENCES

1. Tanoue, T., and Takeichi, M. (2005) New insights into Fat cadherins, *J. Cell Sci. 118*, 2347−2353.
2. Sechi, A. S., and Wehland, J. (2004) ENA/VASP proteins: multifunctional regulators of actin cytoskeleton dynamics, *Front. Biosci. 9*, 1294−1310.
3. Krause, M., Dent, E. W., Bear, J. E., Loureiro, J. J., and Gertler, F. B. (2003) Ena/VASP proteins: regulators of the actin cytoskeleton and cell migration, *Annu. Rev. Cell Dev. Biol. 19*, 541−564.
4. Kwiatkowski, A. V., Gertler, F. B., and Loureiro, J. J. (2003) Function and regulation of Ena/VASP proteins, *Trends Cell Biol. 13*, 386−392.
5. Renfranz, P. J., and Beckerle, M. C. (2002) Doing (F/L)PPPPs: EVH1 domains and their proline-rich partners in cell polarity and migration, *Curr. Opin. Cell Biol. 14*, 88−103.
6. Bear, J. E., Krause, M., and Gertler, F. B. (2001) Regulating cellular actin assembly, *Curr. Opin. Cell Biol. 13*, 158−166.
7. Meyer, G., and Feldman, E. L. (2002) Signaling mechanisms that regulate actin-based motility processes in the nervous system, *J. Neurochem. 83*, 490−503.
8. Koleske, A. J. (2003) Do filopodia enable the growth cone to find its way, *Sci. STKE 2003*, pe20.
9. Haffner, C., Jarchau, T., Reinhard, M., Hoppe, J., Lohmann, S. M., and Walter, U. (1995) Molecular-cloning, structural-analysis and functional expression of the proline-rich focal adhesion and microfilament-associated protein Vasp, *EMBO J. 14*, 19−27.
10. Gertler, F. B., Doctor, J. S., and Hoffmann, F. M. (1990) Genetic suppression of mutations in the Drosophila Abl protooncogene homolog, *Science 248*, 857−860.
11. Gertler, F. B., Niebuhr, K., Reinhard, M., Wehland, J., and Soriano, P. (1996) Mena, a relative of VASP and Drosophila enabled, is implicated in the control of microfilament dynamics, *Cell 87*, 227−239.
12. Halbrugge, M., and Walter, U. (1989) Purification of a vasodilator-regulated phosphoprotein from human platelets, *Eur. J. Biochem. 185*, 41−50.
13. Ball, L. J., Jarchau, T., Oschkinat, H., and Walter, U. (2002) EVH 1 domains: structure, function and interactions, *FEBS Lett. 513*, 45−52.
14. Harbeck, B., Huttelmaier, S., Schluter, K., Jockusch, B. M., and Illenberger, S. (2000) Phosphorylation of the vasodilator-stimulated phosphoprotein regulates its interaction with actin, *J. Biol. Chem. 275*, 30817−30825.
15. Eigenthaler, M., Nolte, C., Halbrugge, M., and Walter, U. (1992) Concentration and regulation of cyclic nucleotides, cyclic-nucleotide-dependent protein kinases and one of their major substrates in human platelets. Estimating the rate of cAMP-regulated and cGMP-regulated protein phosphorylation in intact cells, *Eur. J. Biochem. 205*, 471−481.
16. Butt, E., Abel, K., Krieger, M., Palm, D., Hoppe, V., Hoppe, J., and Walter, U. (1994) cAMP- and cGMP-dependent protein kinase phosphorylation sites of the focal adhesion vasodilator-stimulated phosphoprotein (VASP) in vitro and in intact human platelets, *J. Biol. Chem. 269*, 14509−14517.
17. Chitaley, K., Chen, L., Galler, A., Walter, U., Daum, G., and Clowes, A. W. (2004) Vasodilator-stimulated phosphoprotein is a substrate for protein kinase C, *FEBS Lett. 556*, 211−215.
18. Krugmann, S., Jordens, I., Gevaert, K., Driessens, M., Vandekerckhove, J., and Hall, A. (2001) Cdc42 induces filopodia by promoting the formation of an IRSp53:Mena complex, *Curr. Biol. 11*, 1645−1655.
19. Ahern-Djamali, S. M., Bachmann, C., Hua, P., Reddy, S. K., Kastenmeier, A. S., Walter, U., and Hoffmann, F. M. (1999) Identification of profilin and src homology 3 domains as binding partners for Drosophila enabled, *Proc. Natl. Acad. Sci. U.S.A. 96*, 4977−4982.
20. Russo, T., Faraonio, R., Minopoli, G., De Candia, P., De Renzis, S., and Zambrano, N. (1998) Fe65 and the protein network centered around the cytosolic domain of the Alzheimer's β-amyloid precursor protein, *FEBS Lett. 434*, 1−7.
21. Reinhard, M., Giehl, K., Abel, K., Haffner, C., Jarchau, T., Hoppe, V., Jockusch, B. M., and Walter, U. (1995) The proline-rich focal adhesion and microfilament protein VASP is a ligand for profilins, *EMBO J. 14*, 1583−1589.
22. Zimmermann, J., Labudde, D., Jarchau, T., Walter, U., Oschkinat, H., and Ball, L. J. (2002) Relaxation, equilibrium oligomerization, and molecular symmetry of the VASP (336−380) EVH2 tetramer, *Biochemistry 41*, 11143−11151.
23. Tani, K., Sato, S., Sukezane, T., Kojima, H., Hirose, H., Hanafusa, H., and Shishido, T. (2003) Abl interactor 1 promotes tyrosine 296 phosphorylation of mammalian enabled (Mena) by c-Abl kinase, *J. Biol. Chem. 278*, 21685−21692.
24. Walders-Harbeck, B., Khaitlina, S. Y., Hinssen, H., Jockusch, B. M., and Illenberger, S. (2002) The vasodilator-stimulated phosphoprotein promotes actin polymerisation through direct binding to monomeric actin, *FEBS Lett. 529*, 275−280.
25. Bachmann, C., Fischer, L., Walter, U., and Reinhard, M. (1999) The EVH2 domain of the vasodilator-stimulated phosphoprotein mediates tetramerization, F-actin binding, and actin bundle formation, *J. Biol. Chem. 274*, 23549−23557.
26. Kuhnel, K., Jarchau, T., Wolf, E., Schlichting, I., Walter, U., Wittinghofer, A., and Strelkov, S. V. (2004) The VASP tetramerization domain is a right-handed coiled coil based on a 15-residue repeat, *Proc. Natl. Acad. Sci. U.S.A. 101*, 17027−17032.
27. Sparks, A. B., Rider, J. E., Hoffman, N. G., Fowlkes, D. M., Quillam, L. A., and Kay, B. K. (1996) Distinct ligand preferences of Src homology 3 domains from Src, Yes, Abl, Cortactin, p53bp2, PLCgamma, Crk, and Grb2, *Proc. Natl. Acad. Sci. U.S.A. 93*, 1540−1544.
28. Yu, H., Chen, J. K., Feng, S., Dalgarno, D. C., Brauer, A. W., and Schreiber, S. L. (1994) Structural basis for the binding of proline-rich peptides to SH3 domains, *Cell 76*, 933−945.
29. Macias, M. J., Wiesner, S., and Sudol, M. (2002) WW and SH3 domains, two different scaffolds to recognize proline-rich ligands, *FEBS Lett. 513*, 30−37.
30. Chen, H. I., and Sudol, M. (1995) The WW domain of Yes-associated protein binds a proline-rich ligand that differs from the consensus established for Src homology 3-binding modules, *Proc. Natl. Acad. Sci. U.S.A. 92*, 7819−7823.
31. Macias, M. J., Hyvonen, M., Baraldi, E., Schultz, J., Sudol, M., Saraste, M., and Oschkinat, H. (1996) Structure of the WW domain of a kinase-associated protein complexed with a proline-rich peptide, *Nature 382*, 646−649.
32. Nishizawa, K., Freund, C., Li, J., Wagner, G., and Reinherz, E. L. (1998) Identification of a proline-binding motif regulating CD2-triggered T lymphocyte activation, *Proc. Natl. Acad. Sci. U.S.A. 95*, 14897−14902.
33. Freund, C., Dotsch, V., Nishizawa, K., Reinherz, E. L., and Wagner, G. (1999) The GYF domain is a novel structural fold that is involved in lymphoid signaling through proline-rich sequences, *Nat. Struct. Biol. 6*, 656−660.
34. Pornillos, O., Alam, S. L., Davis, D. R., and Sundquist, W. I. (2002) Structure of the Tsg101 UEV domain in complex with the PTAP motif of the HIV-1 p6 protein, *Nat. Struct. Biol. 9*, 812−817.
35. Pornillos, O., Alam, S. L., Rich, R. L., Myszka, D. G., Davis, D. R., and Sundquist, W. I. (2002) Structure and functional interactions of the Tsg101 UEV domain, *EMBO J. 21*, 2397−2406.
36. Schutt, C. E., Myslik, J. C., Rozycki, M. D., Goonesekere, N. C., and Lindberg, U. (1993) The structure of crystalline profilin-β-actin, *Nature 365*, 810−816.
37. Mahoney, N. M., Janmey, P. A., and Almo, S. C. (1997) Structure of the profilin-poly-L-proline complex involved in morphogenesis and cytoskeletal regulation, *Nat. Struct. Biol. 4*, 953−960.
38. Mahoney, N. M., Rozwarski, D. A., Fedorov, E., Fedorov, A. A., and Almo, S. C. (1999) Profilin binds proline-rich ligands in two distinct amide backbone orientations, *Nat. Struct. Biol. 6*, 666−671.

39. Zarrinpar, A., Bhattacharyya, R. P., and Lim, W. A. (2003) The structure and function of proline recognition domains, *Sci. STKE 2003*, re8-.
40. Ball, L. J., Kuhne, R., Schneider-Mergener, J., and Oschkinat, H. (2005) Recognition of proline-rich motifs by protein-protein-interaction domains, *Angew. Chem., Int. Ed. Engl. 44*, 2852−2869.
41. Volkman, B. F., Prehoda, K. E., Scott, J. A., Peterson, F. C., and Lim, W. A. (2002) Structure of the N-WASP EVH1 domain-WIP complex: Insight into the molecular basis of Wiskott-Aldrich Syndrome, *Cell 111*, 565−576.
42. Prehoda, K. E., Lee, D. J., and Lim, W. A. (1999) Structure of the Enabled/VASP homology 1 domain-peptide complex: a key component in the spatial control of actin assembly, *Cell 97*, 471−480.
43. Harmer, N. J., Sivak, J. M., Amaya, E., and Blundell, T. L. (2005) 1.15 angstrom crystal structure of the X-tropicalis Spred1 EVH1 domain suggests a fourth distinct peptide-binding mechanism within the EVH1 family, *FEBS Lett. 579*, 1161−1166.
44. Beneken, J., Tu, J. C., Xiao, B., Nuriya, M., Yuan, J. P., Worley, P. F., and Leahy, D. J. (2000) Structure of the Homer EVH1 domain-peptide complex reveals a new twist in polyproline recognition, *Neuron 26*, 143−154.
45. Fedorov, A. A., Fedorov, E., Gertler, F., and Almo, S. C. (1999) Structure of EVH1, a novel proline-rich ligand-binding module involved in cytoskeletal dynamics and neural function, *Nat. Struct. Biol. 6*, 661−665.
46. Ball, L. J., Kuhne, R., Hoffmann, B., Hafner, A., Schmieder, P., Volkmer-Engert, R., Hof, M., Wahl, M., Schneider-Mergener, J., Walter, U., Oschkinat, H., and Jarchau, T. (2000) Dual epitope recognition by the VASP EVH1 domain modulates polyproline ligand specificity and binding affinity, *EMBO J. 19*, 4903−4914.
47. Rutledge, S., Chin, J., and Schepartz, A. (2002) A view to a kill: ligands for Bcl-2 family proteins, *Curr. Opin. Chem. Biol. 6*, 479−485.
48. Gemperli, A. C., Rutledge, S. E., Maranda, A., and Schepartz, A. (2005) Paralog-selective ligands for Bcl-2 proteins, *J. Am. Chem. Soc. 127*, 1596−1597.
49. Rutledge, S. E., Volkman, H. M., and Schepartz, A. (2003) Molecular recognition of protein surfaces: high affinity ligands for the CBPKIX domain, *J. Am. Chem. Soc. 125*, 14336−14347.
50. Volkman, H. M., Rutledge, S. E., and Schepartz, A. (2005) Binding mode and transcriptional activation potential of high affinity ligands for the CBPKIX domain, *J. Am. Chem. Soc. 127*, 4649−4658.
51. Kritzer, J. A., Zutshi, R., Cheah, M., Ran, F. A., Webman, R., Wongjirad, T. M., and Schepartz, A. (2006) Miniature protein inhibitors of the p53-hDM2 interaction, *ChemBioChem 7*, 29−31.
52. Chin, J. W., and Schepartz, A. (2001) Design and evolution of a miniature Bcl-2 binding protein, *Angew. Chem., Int. Ed. Engl. 40*, 3806−3809.
53. Chin, J. W., and Schepartz, A. (2001) Concerted evolution of structure and function in a miniature protein, *J. Am. Chem. Soc. 123*, 2929−2930.
54. Yang, L., and Schepartz, A. (2005) Relationship between folding and function in a sequence-specific miniature DNA-binding protein, *Biochemistry 44*, 7469−7478.
55. Montclare, J. K., and Schepartz, A. (2003) Miniature homeodomains: high specificity without an N-terminal arm, *J. Am. Chem. Soc. 125*, 3416−3417.
56. Schneider, T. L., Mathew, R. S., Rice, K. P., Tamaki, K., Wood, J. L., and Schepartz, A. (2005) Increasing the kinase specificity of k252a by protein surface recognition, *Org. Lett. 7*, 1695−1698.
57. Cobos, E. S., Pisabarro, M. T., Vega, M. C., Lacroix, E., Serrano, L., Ruiz-Sanz, J., and Martinez, J. C. (2004) A miniprotein scaffold used to assemble the polyproline II binding epitope recognized by SH3 domains, *J. Mol. Biol. 342*, 355−365.
58. Weston, C. J., Cureton, C. H., Calvert, M. J., Smart, O. S., and Allemann, R. K. (2004) A stable miniature protein with oxaloacetate decarboxylase activity, *ChemBioChem 5*, 1075−1080.
59. Nicoll, A. J., and Allemann, R. K. (2004) Nucleophilic and general acid catalysis at physiological pH by a designed miniature esterase, *Org. Biomol. Chem. 2*, 2175−2180.
60. Guerrero, L., Smart, O. S., Woolley, G. A., and Allemann, R. K. (2005) Photocontrol of DNA binding specificity of a miniature engrailed homeodomain, *J. Am. Chem. Soc. 127*, 15624−15629.
61. Lasa, I., Gouin, E., Goethals, M., Vancompernolle, K., David, V., Vandekerckhove, J., and Cossart, P. (1997) Identification of two regions in the N-terminal domain of ActA involved in the actin comet tail formation by *Listeria monocytogenes*, *EMBO J. 16*, 1531−1540.
62. Lauer, P., Theriot, J. A., Skoble, J., Welch, M. D., and Portnoy, D. A. (2001) Systematic mutational analysis of the amino-terminal domain of the *Listeria monocytogenes* ActA protein reveals novel functions in actin-based motility, *Mol. Microbiol. 42*, 1163−1177.
63. Samarin, S., Romero, S., Kocks, C., Didry, D., Pantaloni, D., and Carlier, M. F. (2003) How VASP enhances actin-based motility, *J. Cell Biol. 163*, 131−142.
64. Rafelski, S. M., and Theriot, J. A. (2005) Bacterial shape and ActA distribution affect initiation of *Listeria monocytogenes* actin-based motility, *Biophys. J. 89*, 2146−2158.
65. Golemi-Kotra, D., Mahaffy, R., Footer, M. J., Holtzman, J. H., Pollard, T. D., Theriot, J. A., and Schepartz, A. (2004) High affinity, paralog-specific recognition of the Mena EVH1 domain by a miniature protein, *J. Am. Chem. Soc. 126*, 4−5.
66. Theriot, J. A., and Fung, D. C. (1998) *Listeria monocytogenes*-based assays for actin assembly factors, *Methods Enzymol. 298*, 114−122.
67. Nguyen, J. T., Porter, M., Amoui, M., Miller, W. T., Zuckermann, R. N., and Lim, W. A. (2000) Improving SH3 domain ligand selectivity using a non-natural scaffold, *Chem. Biol. 7*, 463−473.
68. Theriot, J. A., Rosenblatt, J., Portnoy, D. A., Goldschmidt-Clermont, P. J., and Mitchison, T. J. (1994) Involvement of profilin in the actin-based motility of *L. monocytogenes* in cells and in cell-free extracts, *Cell 76*, 505−517.
69. Southwick, F. S., and Purich, D. L. (1994) Arrest of *Listeria* movement in host cells by a bacterial ActA analogue: implications for actin-based motility, *Proc. Natl. Acad. Sci. U.S.A. 91*, 5168−5172.
70. Smith, G. A., Theriot, J. A., and Portnoy, D. A. (1996) The tandem repeat domain in the *Listeria monocytogenes* ActA protein controls the rate of actin-based motility, the percentage of moving bacteria, and the localization of vasodilator-stimulated phosphoprotein and profilin, *J. Cell Biol. 135*, 647−660.
71. Niebuhr, K., Ebel, F., Frank, R., Reinhard, M., Domann, E., Carl, U. D., Walter, U., Gertler, F. B., Wehland, J., and Chakraborty, T. (1997) Novel proline-rich motif present in ActA of *Listeria monocytogenes* and cytoskeletal proteins is the ligand for the EVH1 domain, a protein module present in the Ena/VASP family, *EMBO J. 16*, 5433−5444.
72. Zimmermann, J., Kuhne, R., Volkmer-Engert, R., Jarchau, T., Walter, U., Oschkinat, H., and Ball, L. J. (2003) Design of N-substituted peptomer ligands for EVH1 domains, *J. Biol. Chem. 278*, 36810−36818.
73. Laurent, V., Loisel, T. P., Harbeck, B., Wehman, A., Grobe, L., Jockusch, B. M., Wehland, J., Gertler, F. B., and Carlier, M. F. (1999) Role of proteins of the Ena/VASP family in actin-based motility of *Listeria monocytogenes*, *J. Cell Biol. 144*, 1245−1258.
74. Kocks, C., Gouin, E., Tabouret, M., Berche, P., Ohayon, H., and Cossart, P. (1992) *L. monocytogenes*-induced actin assembly requires the actA gene product, a surface protein, *Cell 68*, 521−531.
75. Pistor, S., Chakraborty, T., Walter, U., and Wehland, J. (1995) The bacterial actin nucleator protein ActA of *Listeria monocytogenes* contains multiple binding sites for host microfilament proteins, *Curr. Biol. 5*, 517−525.
76. Smith, G. A., Portnoy, D. A., and Theriot, J. A. (1995) Asymmetric distribution of the *Listeria monocytogenes* ActA protein is required and sufficient to direct actin-based motility, *Mol. Microbiol. 17*, 945−951.
77. Machner, M. P., Urbanke, C., Barzik, M., Otten, S., Sechi, A. S., Wehland, J., and Heinz, D. W. (2001) ActA from *Listeria monocytogenes* can interact with up to four Ena/VASP homology 1 domains simultaneously, *J. Biol. Chem. 276*, 40096−40103.
78. Auerbuch, V., Loureiro, J. J., Gertler, F. B., Theriot, J. A., and Portnoy, D. A. (2003) Ena/VASP proteins contribute to *Listeria monocytogenes* pathogenesis by controlling temporal and spatial persistence of bacterial actin-based motility, *Mol. Microbiol. 49*, 1361−1375.
79. Bear, J. E., Loureiro, J. J., Libova, I., Fassler, R., Wehland, J., and Gertler, F. B. (2000) Negative regulation of fibroblast motility by Ena/VASP proteins, *Cell 101*, 717−728.
80. Jenzora, A., Behrendt, B., Small, J. V., Wehland, J., and Stradal, T. E. (2005) PREL1 provides a link from Ras signalling to the actin cytoskeleton via Ena/VASP proteins, *FEBS Lett. 579*, 455−463.

81. Lafuente, E. M., van Puijenbroek, A. A., Krause, M., Carman, C. V., Freeman, G. J., Berezovskaya, A., Constantine, E., Springer, T. A., Gertler, F. B., and Boussiotis, V. A. (2004) RIAM, an Ena/VASP and Profilin ligand, interacts with Rap1-GTP and mediates Rap1-induced adhesion, *Dev. Cell 7*, 585−595.
82. Krause, M., Leslie, J. D., Stewart, M., Lafuente, E. M., Valderrama, F., Jagannathan, R., Strasser, G. A., Rubinson, D. A., Liu, H., Way, M., Yaffe, M. B., Boussiotis, V. A., and Gertler, F. B. (2004) Lamellipodin, an Ena/VASP ligand, is implicated in the regulation of lamellipodial dynamics, *Dev. Cell 7*, 571−583.
83. Geese, M., Loureiro, J. J., Bear, J. E., Wehland, J., Gertler, F. B., and Sechi, A. S. (2002) Contribution of Ena/VASP proteins to intracellular motility of listeria requires phosphorylation and proline-rich core but not F-actin binding or multimerization, *Mol. Biol. Cell 13*, 2383−2396.
84. Hunke, C., Hirsch, T., and Eichler, J. (2006) Structure-based synthetic mimicry of discontinuous protein binding sites: inhibitors of the interaction of Mena EVH1 domain with proline-rich ligands, *ChemBioChem* 1258−1264.
85. Cram, D. J. (1988) The design of molecular hosts, guests, and their complexes, *Science 240*, 760−767.
86. Wedemayer, G. J., Patten, P. A., Wang, L. H., Schultz, P. G., and Stevens, R. C. (1997) Structural insights into the evolution of an antibody combining site, *Science 276*, 1665−1669.
87. Eaton, B. E., Gold, L., and Zichi, D. A. (1995) Let's get specific: the relationship between specificity and affinity, *Chem. Biol. 2*, 633−638.

BI700975F